Enhanced hole injection and transport in molybdenum-dioxide-doped organic hole-transporting layers

Toshinori Matsushima[1] and Chihaya Adachi[2,1,a)]
[1]*Core Research for Evolutional Science and Technology Program, Japan Science and Technology Agency, 1-32-12 Higashi, Shibuya, Tokyo 150-0011, Japan*
[2]*Center for Future Chemistry, Kyushu University, 744 Motooka, Nishi, Fukuoka 819-0395, Japan*

(Received 14 August 2007; accepted 23 November 2007; published online 1 February 2008)

We have found that molybdenum dioxide (MoO_2) is an excellent dopant for enhancing electrical conductivities in organic hole-transporting layers. We fabricated hole-only devices with an alpha-sexithiophene (α-6T) layer doped with MoO_2 at various concentrations to investigate how doping MoO_2 into the α-6T layers influences the hole-injection and hole-transport characteristics of these layers. We observed a marked increase in electrical conductivity as a result of the MoO_2 doping. The 30-mol % MoO_2-doped α-6T layer had a high electrical conductivity of $8.9 \pm 1.3 \times 10^{-6}$ S/cm. From the results of our visible/near-infrared absorption spectra study of these doped layers, we confirmed that this increase in electrical conductivity is caused by a charge transfer between MoO_2 and α-6T, which leads to an increase in free hole concentration in the doped layers and the formation of an ohmic contact at an electrode/α-6T interface. In the latter part of this paper, we discuss current flow and electroluminescence (EL) characteristics of organic light-emitting diodes (OLEDs) with a 30-mol % MoO_2-doped α-6T hole-transporting layer and a 30-mol % Cs-doped phenyldipyrenylphosphine oxide ($POPy_2$) electron-transporting layer. We achieved an extremely low driving voltage of 3.1 V required for a current density of 100 mA/cm^2 in the doped OLEDs owing to the use of the α-6T and $POPy_2$ layers with high carrier mobilities and the excellent *p*-type MoO_2 and *n*-type Cs dopants. We demonstrated the enhancement of power efficiencies by $\approx$2 times in the doped OLEDs compared with undoped OLEDs and observed bright EL at low driving voltages in the doped OLEDs, for example, 100 cd/m^2 at 2.3 V, 1000 cd/m^2 at 2.7 V, and 10 000 cd/m^2 at 3.3 V. © *2008 American Institute of Physics*. [DOI: 10.1063/1.2836972]

I. INTRODUCTION

Organic light-emitting diodes (OLEDs) have been developed because of their potential for use in cheap, lightweight, mechanically flexible, large display and light source applications.[1–5] One of the most important remaining issues for OLEDs is their high driving voltages. The driving voltages for most OLEDs are still much higher than those for inorganic LEDs. A reduction in driving voltage to the corresponding photon (exciton) energies of fluorescent and phosphorescent organic molecules is crucial to improve their power conversion efficiencies[6] and lifetimes.[7] To overcome the driving voltage problem, strong electron acceptor and donor materials have frequently been used as dopants in organic hole-transporting layers (HTLs) and electron-transporting layers (ETLs) in OLEDs.[6–32] Doping these materials into HTLs and ETLs induces a charge transfer between the host and dopant materials, leading to a marked increase in free carrier concentration in these doped layers and the formation of an ohmic contact at electrode/organic interfaces.[33,34]

The *p*-type dopant materials used in HTLs include ferric trichloride ($FeCl_3$),[8,19] iodide (I),[9] 2,3,5,6-tetrafluoro-7,7,8,8-tetracyanoquinodimethane (F_4-TCNQ),[6,7,10,16,17,20–23,25,26,29,30,33,34] tris (4-bromophenyl) aminium hexachloroantimonate,[12,13] antimony pentachloride,[15] tungsten trioxide (WO_3),[27] molybdenum trioxide (MoO_3),[28] rhenium dioxide (ReO_2),[31] and carbon-60.[35] The *n*-type dopant materials used in ETLs include lithium (Li),[11,20–22] lithium fluoride (LiF),[14] 4-phenanthridinolato lithium,[18] and cesium (Cs).[6,7,23–27,30,32,34] Furthermore, positive-intrinsic-negative (*p-i-n*) OLEDs using the *p*-type F_4-TCNQ and *n*-type Cs dopants have demonstrated excellent OLED characteristics, such as a high power conversion efficiency of 82 lm/W with an external quantum efficiency of 19.3%,[6] a very long lifetime of 1×10^7 h at 100 cd/m^2,[7] and a low driving voltage of 2.9 V required for a current density of 100 mA/cm^2.[30]

In this study, we found that a transition metal oxide, molybdenum dioxide (MoO_2), is an excellent *p*-type dopant for enhancing electrical conductivities by several orders of magnitude in organic HTLs and lowering driving voltages in OLEDs with a MoO_2-doped HTL. The similar material of MoO_3 has already been used as a *p*-type dopant in HTLs[28] and as a hole-injection layer between an electrode and an HTL.[36–45] We used alpha-sexithiophene (α-6T), whose chemical structure is shown in Fig. 1(a), as a host matrix layer for the MoO_2 dopant because the α-6T layer has excellent hole-transporting properties.[30] We fabricated hole-only devices with the α-6T layer doped with MoO_2 at various concentrations to investigate how doping MoO_2 into the α-6T layers influences the current flow characteristics of these doped layers. We achieved a marked increase in elec-

a)Electronic mail: adachi@cstf.kyushu-u.ac.jp.

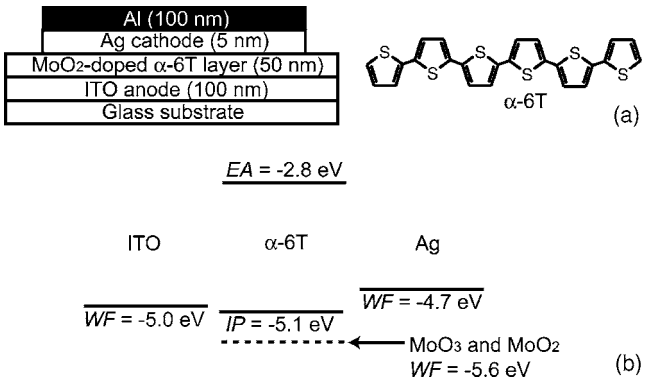

FIG. 1. (a) Schematic of hole-only MoO_2-doped α-6T device structure with high-work-function ITO anode and Ag cathode and chemical structure of α-6T molecule. We varied MoO_2 doping concentrations in α-6T layers from 0 to 100 mol %. α-6T layers doped with MoO_2 at concentrations of 0 and 100 mol % mean pure α-6T and MoO_2 layers, respectively. (b) Energy-level diagram of hole-only MoO_2-doped α-6T devices. The low hole injection barrier of 0.1 eV at the ITO/α-6T interface and high electron injection barrier of 1.9 eV at Ag/α-6T interface provide single carrier injection of holes in these devices.

trical conductivity by a charge transfer between MoO_2 and α-6T. We found that the optimum MoO_2 doping concentration was 30 mol %, providing a very high electrical conductivity of $8.9 \pm 1.3 \times 10^{-6}$ S/cm as well as a high light transmittivity of $93 \pm 2\%$ at a wavelength of 585 nm, where our OLEDs have an electroluminescence (EL) peak maximum, for the MoO_2-doped α-6T layers, which are advantageous for a reduction in driving voltage and a small loss of EL efficiencies in OLEDs. We fabricated *p-i-n* OLEDs with a HTL of 30-mol % MoO_2-doped α-6T and an ETL of 30-mol % Cs-doped phenyldipyrenylphosphine oxide ($POPy_2$). We demonstrated an extremely low driving voltage of 3.1 V at a current density of 100 mA/cm^2 and the enhancement of power conversion efficiencies by ≈ 2 times in the doped OLEDs compared with undoped OLEDs. Understanding the current flow characteristics of MoO_2-doped HTLs and the operation of *p-i-n* OLEDs will be valuable in designing OLEDs with low driving voltages and high EL efficiencies.

II. EXPERIMENTAL

To investigate the current flow mechanisms of the MoO_2-doped α-6T layers, we fabricated hole-only MoO_2-doped α-6T devices. The structure is schematically shown in Fig. 1(a). Glass substrates coated with a 100-nm-thick layer of indium tin oxide (ITO) with a sheet resistance of 25 Ω/sq, purchased from Sanyo Vacuum Industries Co., Ltd., were used for the hole-injecting anode. The substrates were cleaned ultrasonically in a mixture of detergent (Cica clean LX-II, Kanto Chemicals Co.) and pure water (1/10 by volume) for 10 min. This was followed by ultrasonication in pure water for 10 min, acetone for 10 min, and isopropanol for 10 min. The ITO substrates were soaked in boiling isopropanol for 5 min, and placed in an ultraviolet-ozone treatment chamber (UV.TC.NA.003, Bioforce Nanoscience, Inc.) for 20 min. The cleaned ITO substrates were immediately transferred to a vacuum evaporator, which was evacuated to $\approx 10^{-4}$ Pa using a rotary mechanical pump and a turbo molecular pump. At this pressure, a MoO_2-doped α-6T layer was vacuum-deposited on the ITO substrates using coevaporation of MoO_2 and α-6T from resistively heated tantalum boats. The thickness of the MoO_2-doped α-6T layers was precisely set at 50 nm. The MoO_2 doping concentrations in the α-6T layers were controlled to be 0, 2, 10, 20, 30, 40, 50, 60, 70, 80, 90, or 100 mol % using two quartz crystal microbalances. The total coevaporation rate of α-6T and MoO_2 was set to 0.3 nm/s. The α-6T layers doped at the concentrations of 0 and 100 mol % mean pure α-6T and MoO_2 layers, respectively. After the organic layer depositions, the substrates were transferred to a connected vacuum evaporator located next to the organic evaporation chamber without breaking the vacuum. To complete the hole-only devices, a 5-nm-thick high-work-function Ag layer and a 100-nm-thick Al capping layer were successively vacuum-deposited on the doped α-6T layers using resistively heated tungsten boats through a shadow mask to form the bilayer Ag/Al anode layer with an active area of 0.785 mm^2. The evaporation rates were 0.02 nm/s for Ag and 0.1 nm/s for Al. We prepared the MoO_3 and 30-mol % MoO_3-doped α-6T devices with similar device structures using similar vacuum evaporation procedures in order to compare the current flow characteristics of devices doped with MoO_2 and MoO_3. We measured the room-temperature current density–voltage ($J-V$) characteristics of the devices using a semiconductor parameter analyzer (E5250A, Agilent Technologies, Inc.) under a direct current.

To obtain the optical and electronic properties of the α-6T, oxide, and metal layers, we prepared 50-nm-thick α-6T, 1-mol % 4-(dicyanomethylene)-2-methly-6-(*p*-dimethylaminostyryl)-4H-pyran (DCM)-doped tris-(8-hydroxyquinoline) aluminum (Alq_3), MoO_2-doped α-6T, MoO_3-doped α-6T, MoO_2, MoO_3, and Ag films on cleaned quartz substrates using similar preparation conditions to those described earlier. To prepare the DCM-doped Alq_3 film, we used a total evaporation rate of 0.3 nm/s, a pressure of $\approx 10^{-4}$ Pa inside the vacuum evaporator, and resistively heated tantalum boats.

We measured the ionization potential energy (IP) of the α-6T film and the work functions (WFs) of the MoO_2, MoO_3, Ag, and ITO films using an AC-1 ultraviolet photoelectron spectroscope (Rikenkeiki Co). The measured values were IP=−5.1 eV for α-6T, WF=−5.6 eV for MoO_2 and MoO_3, WF=−4.7 eV for Ag, and WF=−5.0 eV for ITO. We calculated the electron affinity (EA) of the α-6T film to be EA=−2.8 eV by subtracting its optical absorption onset energy (energy gap) from the IP value. The energy-level diagram of the hole-only devices with these IP, EA, and WF values is shown in Fig. 1(b).

We measured the visible (VIS) transmittance and VIS/near-infrared (NIR) absorption spectra of the α-6T, MoO_2-doped α-6T, MoO_3-doped α-6T, MoO_2, and MoO_3 films using a spectrophotometer (UV-2550, Shimazu Co.) at room temperature.

We measured the photoluminescence (PL) spectrum and the absolute PL quantum efficiency of the DCM-doped Alq_3 film with a spectrofluorometer (FP-6500-A-ST, Jasco Co., Ltd.) and an integrating sphere system (C9920–02,

Hamamatsu Photonics Co., Ltd.),[46] respectively. The PL spectrum was measured at an excitation light wavelength of 390 nm, where the absorption of Alq_3 molecules is maximum while the absorption of DCM molecules is relatively small. The measured absolute PL quantum efficiency of the 1-mol % DCM-doped Alq_3 film was $74 \pm 2\%$.

We fabricated the OLEDs according to the following steps. 40-nm-thick α-6T,[30] 10-nm-thick *N-N'*-diphenyl-*N-N'*-bis(1-naphthyl)-1,1'-biphenyl-4,4'-diamine (α-NPD), 30-nm-thick 1-mol % DCM-doped Alq_3,[47] and 20-nm-thick $POPy_2$ layers[24] were successively vacuum-deposited on the cleaned ITO substrates using resistively heated tantalum boats at a base pressure of $\approx 10^{-4}$ Pa in the similar vacuum evaporator. The α-6T, DCM-doped Alq_3, and $POPy_2$ layers served as a HTL, an emitting layer, and an ETL, respectively. The evaporation rate of each organic layer was set to 0.3 nm/s. We used the large-energy-gap α-NPD layer (2.9 eV) between the α-6T and DCM-doped Alq_3 layers to block electrons at the α-NPD/Alq_3 interface as well as to prevent energy transfer from the molecules of the large-energy gap Alq_3 (2.6 eV) to those of the small-energy-gap α-6T (2.3 eV).[30] We doped the α-6T and $POPy_2$ layers with MoO_2 and Cs, respectively, at the optimized doping concentration of 30 mol %.[24] This produced an increase in electrical conductivity in the doped layers as a result of a charge transfer between the host and guest materials. To complete the OLEDs, a 100-nm-thick MgAg (Mg/Ag=10/1 by weight)[48] or Al layer was deposited on top of the $POPy_2$ layers through a shadow mask with circular openings to form the metal cathode layer with an active device area of 0.785 mm^2. The evaporation rates were 0.33 nm/s for MgAg and 0.1 nm/s for Al. Current density–voltage–external quantum efficiency ($J-V-\eta_{ext}$) characteristics of the OLEDs were simultaneously measured with an E5250A semiconductor parameter analyzer and a calibrated silicon photodiode (1930-C, Newport Co.) at room temperature under a direct current. The luminance (L) was calculated from η_{ext} assuming a Lambertian emission pattern. The EL spectra of these OLEDs were measured with a spectrometer (SD-2000, Ocean Optics, Inc.) at a constant current density of 100 mA/cm^2.

III. RESULTS AND DISCUSSION

A. $J-V$ characteristics of MoO_2-doped α-6T layers

In this section, we discuss how doping MoO_2 into the α-6T layers influences the $J-V$ characteristics of the doped layers. To make it easy to understand the current flow mechanisms of the MoO_2-doped α-6T layers, we fabricated hole-only MoO_2-doped α-6T devices with high-work-function ITO and Ag electrodes (Fig. 1(a)). As can be seen in the energy-level diagram shown in Fig. 1(b), the work functions of both the ITO (WF=−5.0 eV) anode and Ag (WF=−4.7 eV) cathode were close to the highest occupied molecular orbital level of α-6T (IP=−5.1 eV), and we experimentally confirmed that no EL was observed from the devices, indicating that only holes could be injected in these devices.

The $J-V$ characteristics of the hole-only devices are shown in Fig. 2. They shifted to higher current densities and

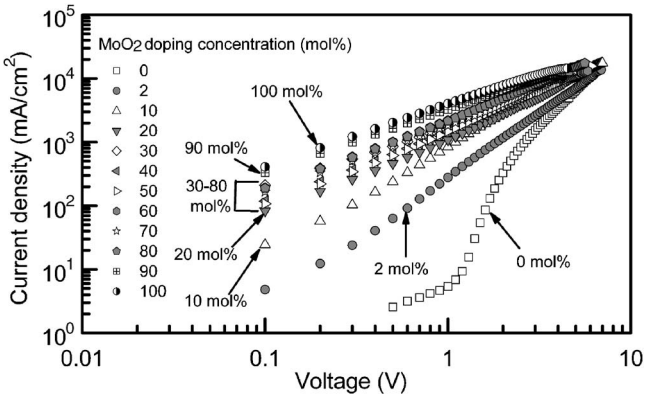

FIG. 2. Current density–voltage characteristics of hole-only MoO_2-doped α-6T devices, whose structure and energy-level diagram are shown in Figs. 1(a) and 1(b), respectively.

gradually became $J \propto V^{1.0}$ as the MoO_2 doping concentrations were increased from 0 to 100 mol %. The α-6T layers doped with MoO_2 at a concentration higher than 20 mol % exhibited $J \propto V^{1.0}$ characteristics, meaning that an ohmic contact was formed at the ITO/α-6T interface. We calculated the electrical conductivities of the doped layers from the $J \propto V^{1.0}$ regions, which are summarized in Table I. The doped layers had high electrical conductivities ranging from 10^{-6} to 10^{-5} S/cm. These enhanced electrical conductivities and the formation of an ohmic contact are attributable to an increase in free hole concentration caused by a charge transfer between α-6T and MoO_2, which is discussed later in Sec. III B.

The current densities at a driving voltage of 2 V, which were estimated from Fig. 2, are plotted as a function of the MoO_2 concentrations in Fig. 3, and these values are also summarized in Table I. We observed two regions where the current densities suddenly increased. The first increase in current density in the low MoO_2 concentration region between 0 and 20 mol % was caused by a charge transfer between α-6T and MoO_2. Since the current densities of the doped layers at concentrations higher than 70 mol % gradually approached that of the pure MoO_2 layer, we can only speculate that a semiconducting MoO_2 network was formed and that current flowed through the MoO_2 network in the highly doped layers. Therefore, the second increase in current density in the high concentration region between 70 and 90 mol % probably originates from both an increase in free hole concentration caused by a charge transfer and the formation of the semiconducting MoO_2 network in the α-6T layers.

Although the enhanced electrical conductivities in the doped layers are advantageous for reducing the driving voltage in OLEDs, doping MoO_2 into the α-6T layers gave rise to the problem of low light transmittivity, meaning that photons generated inside OLEDs were absorbed by the low-light-transmittivity doped layers and the EL efficiencies of OLEDs with these doped layers decreased when the doped layers were used as a HTL in OLEDs. To investigate the light transmittivities of the doped layers, we prepared MoO_2-doped α-6T films on quartz substrates and measured their optical transmittance spectra in the visible region. The light transmittivities of the doped films at a wavelength of

TABLE I. Current densities at driving voltage of 2 V, electrical conductivities, and light transmittivities at EL peak maximum of 585 nm of 50-nm-thick MoO_2-doped α-6T layers

MoO_2 doping concentration (mol %)	Current density at 2 V (mA/cm^2)	Electrical conductivity (S/cm)	Light transmittivity at 585 nm (%)
0 (pure α-6T layer)	300 ± 100	No $J \propto V$ characteristics observed	96 ± 1
2	900 ± 300	No $J \propto V$ characteristics observed	96 ± 2
10	2800 ± 500	No $J \propto V$ characteristics observed	96 ± 2
20	3000 ± 1000	$7.6 \pm 2.5 \times 10^{-6}$	96 ± 2
30	3500 ± 500	$8.9 \pm 1.3 \times 10^{-6}$	93 ± 2
40	3500 ± 900	$8.9 \pm 2.3 \times 10^{-6}$	92 ± 1
50	3600 ± 200	$9.2 \pm 0.5 \times 10^{-6}$	91 ± 2
60	4000 ± 400	$1.0 \pm 0.1 \times 10^{-5}$	88 ± 2
70	4000 ± 1100	$1.0 \pm 0.3 \times 10^{-5}$	87 ± 2
80	4800 ± 300	$1.2 \pm 0.1 \times 10^{-5}$	85 ± 2
90	6400 ± 500	$1.6 \pm 0.1 \times 10^{-5}$	79 ± 2
100 (pure MoO_2 layer)	7800 ± 1200	$2.0 \pm 0.3 \times 10^{-5}$	74 ± 1

585 nm, where the 1-mol % DCM-doped Alq_3 OLEDs had an EL peak maximum, are also plotted in Fig. 3, and these values are also summarized in Table I.

While the electrical conductivities increased, the light transmittivities monotonically decreased as the MoO_2 doping concentrations were increased from 0 to 100 mol %. This decrease in light transmittivity was due to an increase in the MoO_2 component, which has low light transmittivity, in the films. When considering the trade-off between the electrical conductivities and the light transmittivities, we infer that the optimum MoO_2 doping concentration is 30 mol %. The 30-mol % MoO_2-doped α-6T layer had high electrical conductivity of $8.9 \pm 1.3 \times 10^{-6}$ S/cm as well as high light transmittivity of $93 \pm 2\%$, providing a reduction in driving voltage and a small loss of EL efficiency in OLEDs.

B. Comparing $J-V$ characteristics of MoO_3- and MoO_2-doped α-6T layers

A reduction in the driving voltage for OLEDs has also been accomplished by doping the similar material of MoO_3 into an α-NPD HTL in another study reported by Ikeda *et al.*[28] In this section, we discuss whether MoO_2 or MoO_3 is the better dopant for enhancing electrical conductivities of the α-6T layers. To do this, we fabricated hole-only devices with the structure of glass/ITO (150 nm)/pure α-6T, 30-mol % MoO_3-doped α-6T, 30-mol % MoO_2-doped α-6T, pure MoO_3, or pure MoO_2 layer (50 nm)/Ag (5 nm)/Al (100 nm) and investigated the hole-injection and hole-transport characteristics of these devices. The $J-V$ characteristics of the hole-only devices are shown in Fig. 4. The current densities at 2 V estimated from Fig. 4, the electrical conductivities calculated from $J \propto V^{1.0}$ regions in Fig. 4, and the light transmittivities at 585 nm of these layers are summarized in Table II.

We observed a marked increase in current density by doping MoO_2 and MoO_3 into the α-6T layers compared with the undoped α-6T layer, suggesting that both MoO_2 and MoO_3 dopants induce a charge transfer between the dopants and α-6T molecules. The doped α-6T, MoO_2, and MoO_3 layers had $J \propto V^{1.0}$ characteristics. Comparing the $J-V$ characteristics of the MoO_2- and MoO_3-doped α-6T devices, we found that the MoO_2 dopant could provide higher electrical conductivity ($8.9 \pm 1.3 \times 10^{-6}$ S/cm) for the α-6T layer than the MoO_3 dopant could ($6.4 \pm 1.0 \times 10^{-6}$ S/cm). Moreover, these MoO_2- and MoO_3-doped layers had very good 585-nm

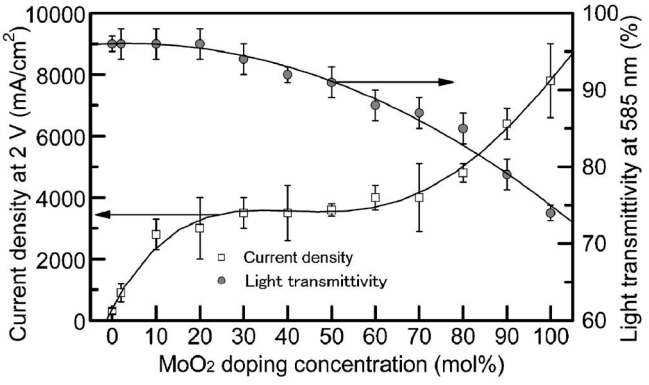

FIG. 3. Current densities at driving voltage of 2 V vs MoO_2 doping concentrations and light transmittivities at a wavelength of 585 nm vs MoO_2 doping concentrations. Current densities at 2 V were estimated from Fig. 2. The wavelength of 585 nm corresponds to that of the EL peak maximum observed in 1-mol % DCM-doped Alq_3 OLEDs.

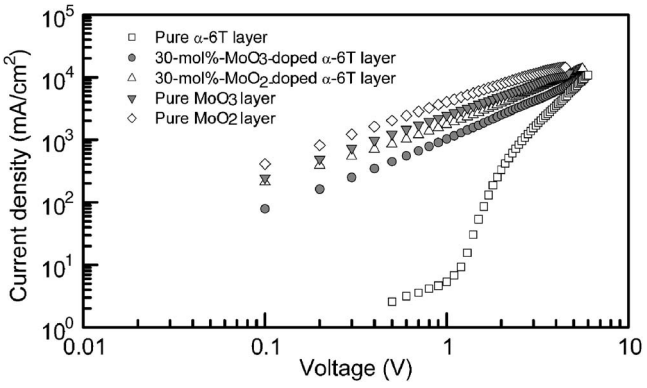

FIG. 4. Current density–voltage characteristics of hole-only devices with the structure of glass/ITO (150 nm)/pure α-6T, 30-mol % MoO_3-doped α-6T, 30-mol % MoO_2-doped α-6T, pure MoO_3, or pure MoO_2 layer (50 nm)/Ag (5 nm)/Al (100 nm).

TABLE II. Current densities at driving voltage of 2 V, electrical conductivities, and light transmittivities at EL peak maximum of 585 nm of 50-nm-thick pure α-6T, 30-mol % MoO_3-doped α-6T, 30-mol % MoO_2-doped α-6T, pure MoO_3, and pure MoO_2 layers.

Sample	Current density at 2 V (mA/cm^2)	Electrical conductivity (S/cm)	Light transmittivity at 585 nm (%)
Pure α-6T layer	300 ± 100	No $J \propto V$ characteristics observed	96 ± 1
30-mol % MoO_3-doped α-6T layer	2500 ± 400	$6.4 \pm 1.0 \times 10^{-6}$	94 ± 2
30-mol % MoO_2-doped α-6T layer	3500 ± 500	$8.9 \pm 1.3 \times 10^{-6}$	93 ± 2
Pure MoO_3 layer	5000 ± 800	$1.3 \pm 0.2 \times 10^{-5}$	80 ± 1
Pure MoO_2 layer	7800 ± 1200	$2.0 \pm 0.3 \times 10^{-5}$	74 ± 1

light transmittivities of $93 \pm 2\%$ and $94 \pm 2\%$, respectively, which is important for reducing the loss of EL efficiencies.

The electrical conductivity of our vacuum-deposited MoO_3 layer was $1.3 \pm 0.2 \times 10^{-5}$ S/cm, which is in the semiconductorlike range and is about seven orders of magnitude lower than that of a radio-frequency magnetron-sputtered MoO_3 layer ($\approx$80 S/cm) with a nearly stoichiometric composition of Mo/O=1/3.[36] We attribute this low electrical conductivity to the compositional difference between the vacuum-deposited and sputtered layers.

To obtain more detailed information about the charge transfer between MoO_2 (or MoO_3) and α-6T molecules, we prepared pure α-6T, 30-mol % MoO_3-doped α-6T, 30-mol % MoO_2-doped α-6T, pure MoO_3, and pure MoO_2 films on quartz substrates and measured the VIS-NIR absorption spectra of these films (Fig. 5).

Although there was no absorption peak at a higher wavelength in the absorption spectra of the undoped α-6T, MoO_2, and MoO_3 films, new broad absorption peaks appeared at around 1200 nm in the absorption spectra of the MoO_2- and MoO_3-doped films. The observation of these new peaks is proof of charge transfer between the dopants and α-6T molecules. Similar charge transfer peaks have been observed in VIS-NIR absorption spectra of organic films doped with I,[9] Li,[11] F_4-TCNQ,[17] $FeCl_3$,[19] Cs,[24] WO_3,[27] MoO_3,[28] and ReO_2.[31]

We found that the charge transfer peak of the MoO_2-doped film was about three times higher in absorbance than that of the MoO_3-doped film, suggesting that a charge transfer between MoO_2 and α-6T can occur more easily than that between MoO_3 and α-6T. Therefore, the

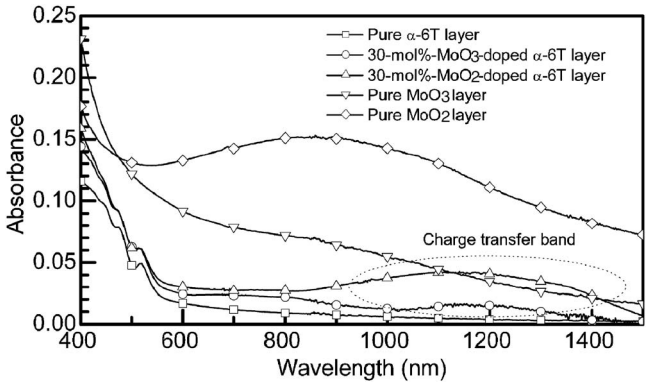

FIG. 5. VIS-NIR absorption spectra of 50-nm-thick pure α-6T, 30-mol % MoO_3-doped α-6T, 30-mol % MoO_2-doped α-6T, pure MoO_3, or pure MoO_2 films prepared on quartz substrates.

MoO_2-doped α-6T layer had higher electrical conductivity than the MoO_3-doped α-6T layer. The deep energy levels (WF=−5.6 eV) of MoO_3 and MoO_2 should enable efficient electron transfer from α-6T to MoO_3 (or MoO_2). We are now striving to understand the difference in the charge transfer and free hole generation mechanisms between the MoO_2- and MoO_3-doped systems.

C. Lowering driving voltages in *p-i-n* OLEDs with MoO_2- and Cs-doped carrier-transporting layers

We fabricated four kinds of the doped OLEDs to confirm the effectiveness of our doping technique. The schematics of the OLED structures (a), (b), (c), and (d) having *p*-type MoO_2 and *n*-type Cs dopants and the chemical structures of $POPy_2$, α-NPD, DCM, and Alq_3 molecules are shown in Fig. 6. We used the high-carrier-mobility α-6T HTL (Ref. 30) and $POPy_2$ ETL (Ref. 24) to reduce the driving voltages in the OLEDs. We doped *p*-type MoO_2 into the α-6T HTLs in (b) and (d) and *n*-type Cs into the $POPy_2$ ETLs in (c) and (d).

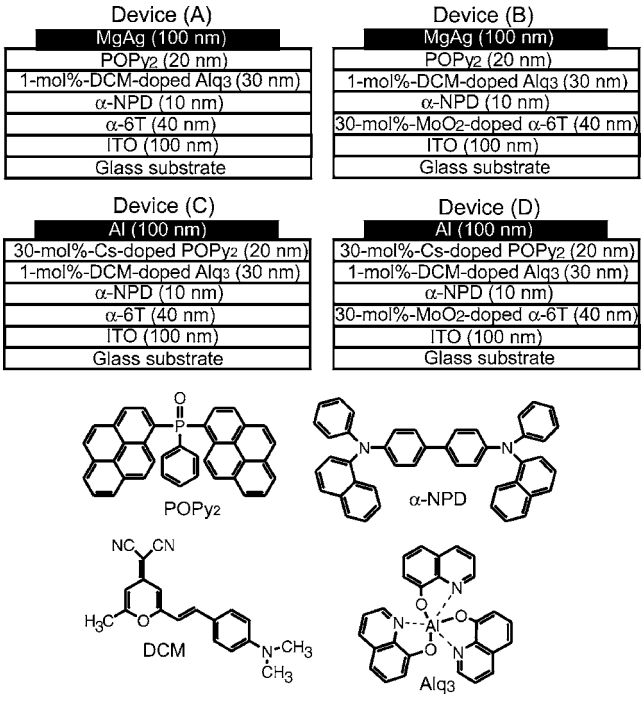

FIG. 6. Schematics of OLEDs structures (a), (b), (c), and (d) and chemical structures of $POPy_2$, α-NPD, DCM, and Alq_3 molecules. MoO_2 was doped into α-6T HTLs in (b) and (d), and Cs was doped into $POPy_2$ ETLs in (c) and (d). Doping concentrations of MoO_2 and Cs in these layers were set to the optimized 30 mol %.

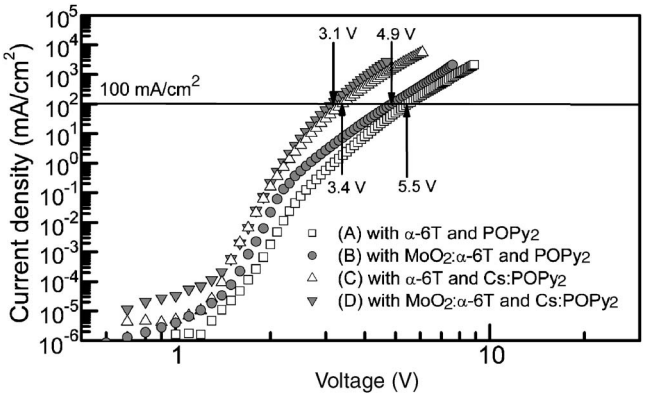

FIG. 7. Current density–voltage characteristics of (a), (b), (c), and (d). Driving voltages required for a current density of 100 mA/cm^2 were 5.5 V for (a), 4.9 V for (b), 3.4 V for (c), and 3.1 V for (d).

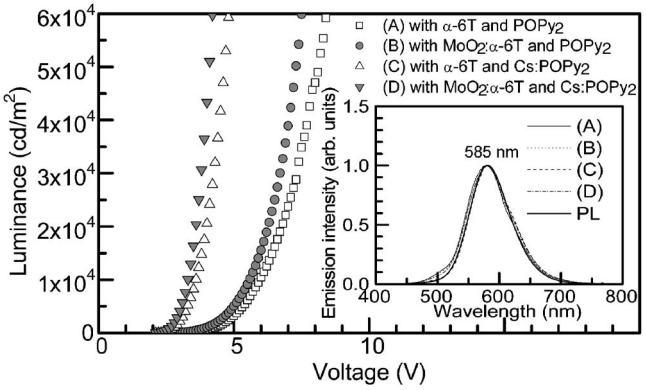

FIG. 8. Luminance–voltage characteristics of (a), (b), (c), and (d). The inset shows EL spectra of (a), (b), (c), and (d), which were operated at constant current density of 100 mA/cm^2, and the PL spectrum of 1-mol % DCM-doped Alq_3 film, which was measured at an excitation light wavelength of 390 nm, where the absorption of Alq_3 is maximum while the absorption of DCM is relatively small.

The doping concentrations of MoO_2 and Cs in these HTLs and ETLs were set to the optimized value of 30 mol %.[24]

The $J-V$ characteristics of (a), (b), (c), and (d) are shown in Fig. 7. The driving voltages required for $J=100$ mA/cm^2 were 5.5 V for (a), 4.9 V for (b), 3.4 V for (c), and 3.1 V for (d), as summarized in Table III. These very low driving voltages resulted from various factors including our use of the following: (1) the high-carrier-mobility α-6T HTL (Ref. 30) and $POPy_2$ ETL (Ref. 24) and (2) the excellent p-type MoO_2 and n-type Cs dopants that can provide a marked increase in electrical conductivity for the doped HTL and ETL by a charge transfer between the dopant and host materials. A driving voltage of 2.9 V at 100 mA/cm^2 was reported in our previous work on a p-i-n OLED with a F_4-TCNQ-doped α-6T HTL and a Cs-doped $POPy_2$ ETL.[30] Since an electron mobility of the $POPy_2$ ETL is probably lower than a hole mobility of the α-6T HTL, we suppose that a voltage drop occurs more predominantly in the $POPy_2$ ETL than in the α-6T HTL. Therefore, the affect of doping the $POPy_2$ ETL with Cs has a bigger impact on the driving voltages of the OLEDs than doping of the α-6T HTL with MoO_2, as shown in Fig. 7.

The charge transfer between dopant and host materials induces an increase in free carrier concentration in doped layers by several orders of magnitude, providing a Fermi level shift and efficient carrier tunneling injection across metal/organic interfaces, i.e., ohmic contacts.[34] Therefore, we did not need a low-work-function metal cathode, such as Ca (Refs. 37 and 38) and MgAg,[47,48] or an electron injection layer, such as LiF (Ref. 49) and Cs_2CO_3,[42,50] between the doped $POPy_2$ and Al layers in (c) and (d).

The $L-V$ characteristics of (a), (b), (c), and (d) are shown in Fig. 8. The driving voltages required for $L=500$ cd/m^2 were 4.0 V for (a), 3.6 V for (b), 2.7 V for (c), and 2.5 V for (d), as summarized in Table III. We observed bright EL in (d) at very low driving voltages, for example, 100 cd/m^2 at 2.3 V, 1000 cd/m^2 at 2.7 V, and 10 000 cd/m^2 at 3.3 V, which are advantageous for low-voltage displays and lighting applications.

The EL spectra of (a), (b), (c), and (d) operated at a constant J of 100 mA/cm^2 and the PL spectrum of a 1-mol % DCM-doped Alq_3 film are shown in the inset of Fig. 8. All the OLEDs exhibited similar EL spectra with a peak maximum of ≈585 nm, which corresponded well with the PL spectrum of a DCM-doped Alq_3 film. No EL arising from the host material, Alq_3, was observed in the EL and PL spectra, suggesting that the Förster energy transfer from the excited-state Alq_3 to ground-state DCM molecules was efficient.[51]

The $\eta_{ext}-J$ and $\eta_{power}-J$ characteristics of (a), (b), (c), and (d) are shown in Fig. 9. At $J=100$ mA/cm^2, we obtained $\eta_{ext}=1.9\%$ and $\eta_{power}=3.5$ lm/W for (a), $\eta_{ext}=1.7\%$ and $\eta_{power}=3.6$ lm/W for (b), $\eta_{ext}=2.0\%$ and $\eta_{power}=5.9$ lm/W for (c), and $\eta_{ext}=2.1\%$ and $\eta_{power}=6.6$ lm/W for (d), as summarized in Table III. The η_{power} was enhanced by ≈2 times by lowering the driving voltages in the OLEDs, while all the OLEDs had almost the same η_{ext}.

We can calculate the theoretical limit of η_{ext} using the simple equation[46] $\eta_{ext}=\eta_{PL}\eta_{out}\eta_{e/h}\eta_{exciton}$, where η_{PL} is the PL quantum efficiency, η_{out} is the light out-coupling effi-

TABLE III. Driving voltages required at current density of 100 mA/cm^2, driving voltages required at luminance of 500 cd/m^2, external quantum efficiencies at current density of 100 mA/cm^2, and power conversion efficiencies at current density of 100 mA/cm^2 of doped OLEDs.

Device	Driving voltage at 100 mA/cm^2 (V)	Driving voltage at 500 cd/m^2 (V)	External quantum efficiency at 100 mA/cm^2 (%)	Power conversion efficiency at 100 mA/cm^2 (lm/W)
(a)	5.5	4.0	1.9	3.5
(b)	4.9	3.6	1.7	3.6
(c)	3.4	2.7	2.0	5.9
(d)	3.1	2.5	2.1	6.6

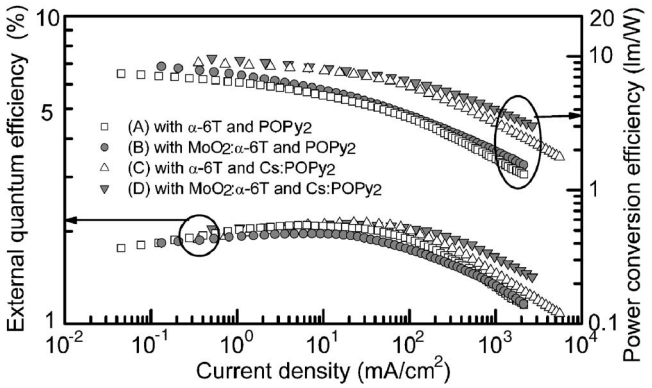

FIG. 9. External quantum efficiency–current density and power conversion efficiency–current density characteristics of (a), (b), (c), and (d).

ciency, $\eta_{e/h}$ is the charge-carrier balance factor, and η_{exciton} is the generation efficiency of singlet or triplet excitons under electrical excitation. The η_{PL} of a 1-mol % DCM-doped Alq_3 film was determined to be $74 \pm 2\%$. Assuming that η_{out} is 20%,[46] $\eta_{e/h}$ is 100%, and η_{exciton} is 25%,[46] the theoretical η_{ext} was calculated to be $3.7 \pm 1\%$ using the equation. From this, one can see that the experimental η_{ext} (2.1%) is lower than the theoretical η_{ext} (3.7%), meaning that the actual $\eta_{e/h}$ is lower than 100%. The experimental η_{ext} and $\eta_{e/h}$ will be improved by carefully adjusting the MoO_2 and Cs doping concentrations or by optimizing OLED structures.

IV. CONCLUSIONS

We investigated how doping MoO_2 into α-6T layers influences the current density–voltage characteristics of the doped α-6T layers. We found that doping MoO_2 into the α-6T layers induced a marked increase in electrical conductivity in these doped layers. This increase in electrical conductivity was caused by a charge transfer between MoO_2 and α-6T, which led to an increase in free hole concentration in the doped layers and efficient hole tunnel injection across metal/organic interfaces. From the results of our VIS-NIR absorption spectra study of the doped layers, we confirmed a charge transfer band peaking at about 1200 nm, which is evidence of a charge transfer between MoO_2 and α-6T. We observed a decrease in light transmittivity in the highly MoO_2-doped α-6T layers, resulting in a loss of EL efficiencies in OLEDs. When considering the electrical conductivities and light transmittivities of the doped layers, we concluded that the optimum MoO_2 doping concentration is 30 mol %. The 30-mol % MoO_2-doped α-6T layer had not only a high electrical conductivity of $8.9 \pm 1.3 \times 10^{-6}$ S/cm, but also a high light transmittivity of $93 \pm 2\%$. We fabricated *p-i-n* OLEDs with a 30-mol % MoO_2-doped α-6T HTL and a 30-mol % Cs-doped $POPy_2$ ETL. We demonstrated an extremely low driving voltage of 3.1 V required for a current density of 100 mA/cm^2 in the doped OLEDs. This low driving voltage resulted from various factors including our use of (1) the high-carrier-mobility α-6T and $POPy_2$ layers and (2) the excellent MoO_2 and Cs dopants that can provide an increase in free carrier concentration for the doped HTL and ETL. The marked reduction in driving voltage in the doped OLEDs enhanced the power efficiencies by ≈ 2 times compared with undoped OLEDs, and bright EL was observed at low driving voltages, for example, 100 cd/m^2 at 2.3 V, 1000 cd/m^2 at 2.7 V, and 10 000 cd/m^2 at 3.3 V.

ACKNOWLEDGMENTS

We thank Shuji Sakamoto and Toshihiro Iwakuma (Idemitsu Kosan Co., Ltd.) for providing us with the hole-transporting material, α-6T, and Seiichiro Murase and Tsuyoshi Tominaga (Toray Industries, Inc.) for providing us with the electron-transporting material, $POPy_2$.

[1] S. R. Forrest, Nature (London) **428**, 911 (2004).
[2] K. Okumoto, H. Kanno, Y. Hamada, H. Takahashi, and K. Shibata, Appl. Phys. Lett. **89**, 063504 (2006).
[3] H. Kanno, N. C. Giebink, Y. Sun, and S. R. Forrest, Appl. Phys. Lett. **89**, 023503 (2006).
[4] H. Kanno, Y. Hamada, K. Nishimura, K. Okumoto, N. Saito, H. Ishida, H. Takahashi, K. Shibata, and K. Mameno, Jpn. J. Appl. Phys., Part 1 **45**, 9219 (2006).
[5] D. Tanaka, H. Sasabe, Y.-J. Li, S.-J. Su, T. Takeda, and J. Kido, Jpn. J. Appl. Phys., Part 2 **46**, L10 (2007).
[6] G. He, M. Pfeiffer, K. Leo, M. Hofmann, J. Birnstock, R. Pudzich, and J. Salbeck, Appl. Phys. Lett. **85**, 3911 (2004).
[7] R. Meerheim, K. Walzer, M. Pfeiffer, and K. Leo, Appl. Phys. Lett. **89**, 061111 (2006).
[8] D. B. Romero, M. Schaer, L. Zuppiroli, B. Cesar, and B. Francois, Appl. Phys. Lett. **67**, 1659 (1995).
[9] F. Huang, A. G. MacDiarmid, and B. R. Hsieh, Appl. Phys. Lett. **71**, 2415 (1997).
[10] J. Blochwitz, M. Pfeiffer, T. Fritz, and K. Leo, Appl. Phys. Lett. **73**, 729 (1998).
[11] J. Kido and T. Matsumoto, Appl. Phys. Lett. **73**, 2866 (1998).
[12] A. Yamamori, C. Adachi, T. Koyama, and Y. Taniguchi, Appl. Phys. Lett. **72**, 2147 (1998).
[13] A. Yamamori, C. Adachi, T. Koyama, and Y. Taniguchi, J. Appl. Phys. **86**, 4369 (1999).
[14] V.-E. Choong, S. Shi, J. Curless, and F. So, Appl. Phys. Lett. **76**, 958 (2000).
[15] C. Ganzorig and M. Fujihara, Appl. Phys. Lett. **77**, 4211 (2000).
[16] X. Zhou, M. Pfeiffer, J. Blochwitz, A. Werner, A. Nollau, T. Fritz, and K. Leo, Appl. Phys. Lett. **78**, 410 (2001).
[17] X. Zhou, J. Blochwitz, M. Pfeiffer, A. Nollau, T. Fritz, and K. Leo, Adv. Funct. Mater. **11**, 310 (2001).
[18] A. Fukase and J. Kido, Jpn. J. Appl. Phys., Part 2 **41**, L334 (2002).
[19] J. Endo, T. Matsumoto, and J. Kido, Jpn. J. Appl. Phys., Part 2 **41**, L358 (2002).
[20] J. Huang, M. Pfeiffer, A. Werner, J. Blochwitz, K. Leo, and S. Liu, Appl. Phys. Lett. **80**, 139 (2002).
[21] M. Pfeiffer, S. R. Forrest, K. Leo, and M. E. Thompson, Adv. Mater. **14**, 1633 (2002).
[22] J. Huang, J. Blochwitz-Nimoth, M. Pfeiffer, and K. Leo, J. Appl. Phys. **93**, 838 (2003).
[23] G. He, O. Schneider, D. Qin, X. Zhou, M. Pfeiffer, and K. Leo, J. Appl. Phys. **95**, 5773 (2004).
[24] T. Oyamada, H. Sasabe, C. Adachi, S. Murase, T. Tominaga, and C. Maeda, Appl. Phys. Lett. **86**, 033503 (2005).
[25] T.-Y. Cho, C.-L. Lin, and C.-C. Wu, Appl. Phys. Lett. **88**, 111106 (2006).
[26] C.-L. Lin, T.-Y. Cho, C.-H. Chang, and C.-C. Wu, Appl. Phys. Lett. **88**, 081114 (2006).
[27] C.-C. Chang, M.-T. Hsieh, J.-F. Chen, S.-W. Hwang, and C. H. Chen, Appl. Phys. Lett. **89**, 253504 (2006).
[28] H. Ikeda, J. Sakata, M. Hayakawa, T. Aoyama, T. Kawakami, K. Kamata, Y. Iwaki, S. Seo, Y. Noda, R. Nomura, and S. Yamazaki, 2006 Society for Information Display International Symposium, Digest of Technical Papers, San Francisco, CA, 2006, p. 923.
[29] J. Guo, N. Koch, S. L. Bernasek, and J. Schwartz, Chem. Phys. Lett. **426**, 370 (2006).
[30] T. Matsushima and C. Adachi, Appl. Phys. Lett. **89**, 253506 (2006).
[31] D.-S. Leem, H.-D. Park, J.-W. Kang, J.-H. Lee, J. W. Kim, and J.-J. Kim, Appl. Phys. Lett. **91**, 011113 (2007).

[32]S. Watanabe, N. Ide, and J. Kido, Jpn. J. Appl. Phys., Part 1 **46**, 1186 (2007).
[33]M. Pfeiffer, A. Beyer, T. Fritz, and K. Leo, Appl. Phys. Lett. **73**, 3202 (1998).
[34]J. Blochwitz, T. Fritz, M. Pfeiffer, K. Leo, D. M. Alloway, P. A. Lee, and N. R. Armstrong, Org. Electron. **2**, 97 (2001).
[35]J. Y. Lee and J. H. Kwon, Appl. Phys. Lett. **88**, 183502 (2006).
[36]S. Tokito, K. Noda, and Y. Taga, J. Phys. D **29**, 2750 (1996).
[37]K. J. Reynolds, J. A. Barker, N. C. Greenham, R. H. Friend, and G. L. Frey, J. Appl. Phys. **92**, 7556 (2002).
[38]G. L. Frey, K. J. Reynolds, and R. H. Friend, Adv. Mater. **14**, 265 (2002).
[39]T. Miyashita, S. Naka, H. Okada, and H. Onnagawa, Jpn. J. Appl. Phys., Part 1 **44**, 3682 (2005).
[40]H. Shimada, S. Naka, H. Okada, and H. Onnagawa, Jpn. J. Appl. Phys., Part 1 **44**, 2830 (2005).
[41]C.-W. Chu, S.-H. Li, C.-W. Chen, V. Shrotriya, and Y. Yang, Appl. Phys. Lett. **87**, 193508 (2005).
[42]C.-W. Chen, Y.-J. Lu, C.-C. Wu, E. H.-E. Wu, C.-W. Chu, and Y. Yang, Appl. Phys. Lett. **87**, 241121 (2005).
[43]V. Shrotriya, G. Li, Y. Yao, C.-W. Chu, and Y. Yang, Appl. Phys. Lett. **88**, 073508 (2006).
[44]R. Satoh, S. Naka, M. Shibata, H. Okada, H. Onnagawa, T. Miyabayashi, and T. Inoue, Jpn. J. Appl. Phys., Part 1 **45**, 1829 (2006).
[45]H. You, Y. Dai, Z. Zhang, and D. Ma, J. Appl. Phys. **101**, 026105 (2007).
[46]Y. Kawamura, H. Sasabe, and C. Adachi, Jpn. J. Appl. Phys., Part 1 **43**, 7729 (2004).
[47]C. W. Tang, S. A. VanSlyke, and C. H. Chen, J. Appl. Phys. **65**, 3610 (1989).
[48]C. W. Tang and S. A. VanSlyke, Appl. Phys. Lett. **51**, 913 (1987).
[49]L. S. Hung, C. W. Tang, and M. G. Mason, Appl. Phys. Lett. **70**, 152 (1997).
[50]T. Hasegawa, S. Miura, T. Moriyama, T. Kimura, I. Takaya, Y. Osato, and H. Mizutani, 2004 Society for Information Display International Symposium, Digest of Technical Papers, Seattle, WA, 2004, p. 154.
[51]V. G. Kozlov, V. Bulović, P. E. Burrows, and S. R. Forrest, Nature (London) **389**, 362 (1997).